Available online at www.sciencedirect.com
SCIENCE DIRECT
Chemical Physics 321 (2006) 171–182
Chemical Physics
www.elsevier.com/locate/chemphys

VUV photophysics of acetic acid: Fragmentation, fluorescence and ionization in the 6–23 eV region

Sydney Leach [a,*], Martin Schwell [b], Hans-Werner Jochims [c], Helmut Baumgärtel [c]

[a] LERMA – UMR 8112, Observatoire de Paris-Meudon, 5, place Jules Janssen, 92195 Meudon, France
[b] Laboratoire Interuniversitaire des Systèmes Atmosphériques (LISA), Université Paris 7 et 12, 61 Avenue du Général de Gaulle, 94010 Creteil Cedex, France
[c] Institut für Physikalische und Theoretische Chemie der Freien Universität Berlin, Takustr. 3, 14195 Berlin, Germany

Received 10 June 2005; accepted 18 August 2005
Available online 28 September 2005

Abstract

VUV photodissociation of gaseous acetic acid was studied in the 6–23 eV range using synchrotron radiation excitation, photofragment fluorescence spectroscopy and mass spectrometry. OH (A-X), CH (A,B-X) and H-Balmer emissions were observed. Their relative intensities were studied by fluorescence excitation spectroscopy. The fluorescence quantum yield for OH emission has a maximum of 0.9% at 13.3 eV photoexcitation, dropping to 0.5% at 20 eV; that for CH (A-X) is 0.35% at 16 eV and 0.4% at 20 eV. Photoionization mass spectra (PIMS) of CH_3COOH were measured and the appearance energies of the principal photoions were determined. IE(CH_3-COOH) = 10.58 ± 0.02 eV is 40–60 meV lower than previous PIMS values. Dissociative ionization reaction channels are discussed in detail. The results call into question previous determinations of the heat of formation and ionization energy of the acetyl radical. A new pathway is suggested for the formation of HCO^+, and the assignments of the $m/z = 16$, 28 and 31 ions are clarified. The formation of CH_3^+ at threshold is shown to involve carbon–carbon bond rupture and a potential energy barrier. The results of this study are used to discuss aspects of astrophysical observations involving the parent and fragment species.

1. Introduction

Absorption of VUV photons by a molecule opens up many photophysical processes, including a variety of relaxation processes [1]. Previous studies of the vacuum-UV (VUV) spectroscopy and photophysics of acetic acid (CH_3COOH) have been mainly limited to absorption and fluorescence measurements below 11.4 eV [2,3], apart from a photoionization mass spectrometric study by Villem and Akopyan [4] up to 13 eV, and one by Zha et al. [5], up to 17 eV.

Photodissociation and dissociative photoionization processes [1] can give rise to electronically and/or vibrationally excited product species, as we found for acetic acid. This molecule is observed in the interstellar medium [6] and is expected to exist in comets [7] where, in both cases, VUV radiation is present. It is also a constituent of the Earth's atmosphere, especially over urban areas [8]. Thus, a study of the VUV photophysics of acetic acid is necessary for interpreting the relevant astrophysical and atmospheric observations.

We have carried out extensive studies on the spectroscopy and photophysics of acetic acid in the 6–23 eV energy region. An analysis of the 6–20 eV photoabsorption spectrum has been made and is published elsewhere [9]. In the present work we have used photofragment fluorescence spectroscopy as an analytical tool to provide insight into the photoprocesses of acetic acid. Identification of the emission features observed in the dispersed fluorescence spectra of CH_3COOH is followed by a fluorescence excitation (FEX) spectral study of the excitation energy dependence of these features. Analysis of the FEX spectra is made with the aid of data from the VUV absorption spectra and thermochemical limit calculations of the relevant processes forming the emitting electronic states. In Table

* Corresponding author. Tel.: +33 0 145077561; fax: +33 0 145077100.
E-mail address: sydney.leach@obspm.fr (S. Leach).

0301-0104/$ - see front matter © 2005 Elsevier B.V. All rights reserved.
doi:10.1016/j.chemphys.2005.08.020

Table 1
Heats of formation (298 K) of species used to calculate thermochemical energies

Species	Heat of formation (298 K) eV	Species	Heat of formation (298 K) eV
H	2.259 [18]	$COOH^+$	6.188 [18]
O	2.58 [18]	HCOO	−1.344 [22]
OH	0.404 [18]	CH_4	−0.772 [19]
OH^+	13.424 [18]	CH_4^+	11.731 [19]
CH	6.174 [19]	CH_3O	0.176 [18]
CO	−1.145 [18]	CH_3O^+	8.725 [19]
CO^+	12.87 [18]	CH_2OH	−0.195 [20]
H_2O	−2.506 [18]	CH_2OH^+	7.343 [20]
HCO	0.436 [20]	CH_2CO^+	9.119 [18]
HCO^+	8.56 [19]	CH_3OH	−2.088 [18]
COH	−0.179 [5]	CH_3OO	0.2083 [23]
COH^+	9.98 [19]	CH_3CO	−0.124 [18]
CO_2	−4.078 [18]	CH_3CO^+	6.876 [18], [19]
CO_2^+	9.693 [18]	CH_3COO	−2.242 [24]
CH_3	1.513 [18]	CH_3COOH	−4.479 [18]
CH_3^+	11.342 [20]	CH_3COOH^+	6.101 [18][a]
COOH (HOCO)	−2.311 [21]		

[a] And present work value of ionization energy of CH_3COOH.

1 are given the heats of formation at 298 K of the atomic or molecular species used to calculate thermochemical threshold energies of the various dissociation processes discussed in the present work. We have also measured, and interpreted, the mass spectra of CH_3OOH as a function of photon excitation energy up to 100 eV, and measured the appearance energies of the ionic products of dissociative ionization. The dissociation reaction channels are discussed in detail. The results of this study are used to discuss aspects of astrophysical observations involving this species.

2. Experimental

Monochromatized synchrotron radiation was obtained from the Berlin electron storage ring BESSY I (multibunch mode) in association with a 1.5 m McPherson monochromator (Normal incidence (NIM), dispersion 5.6 Å/mm). Some of the mass spectrometric measurements were performed at LURE/Orsay (SA63 beamline, 3 m NIM monochromator).

The grating transmission function of the BESSY I monochromator is recorded by detecting the visible fluorescence emitted by the sodium salicylate layer placed on a quartz window. For fluorescence measurements, the synchrotron light beam is focused into an open brass cell, differentially pumped, containing acetic acid vapor at a pressure typically around 10^{-3} mbar. In this pressure region the concentration of acetic acid dimers to monomers is negligibly small [3]. Fluorescence induced in the irradiated target molecules passes through a quartz window and is dispersed using a 20 cm focal length secondary monochromator (Jobin-Yvon H 20 UV, grating blazed at 300 nm). This monochromator has a fixed, exchangeable exit slit but has no entrance slit. The width of the effective "entrance slit" is given by the spatial extension of the exciting light beam (approximately 1 mm). The emitted fluorescence light, measured in the 250–550 nm wavelength range, is detected by a photon-counting Hamamatsu R6060 photomultiplier, cooled to 250 K by a Peltier element. The spectral response function of this arrangement has been determined by recording the spectrum emitted by a tungsten halogen lamp, which is then deconvoluted according to Planck's law. A dispersed fluorescence spectrum typically contains 2 points per nm. The resolution of these spectra is between 4 and 20 nm depending on the choice of the effective exit slit width.

Dispersed fluorescence measurements were carried out at six excitation energies, respectively, 10, 13, 15, 16.2, 18 and 20 eV. The excitation bandwidth was ≈0.8 nm. In recording the fluorescence excitation (FEX) spectra, the secondary monochromator is fixed at a desired wavelength with a large exit slit and the primary monochromator is tuned in steps of typically 50–100 meV (400–800 cm^{-1}). The FEX spectra are corrected for the grating transmission function of the primary monochromator and for the VUV photon flux, respectively. The bandwidth was ≈0.3 nm, and the FEX spectral resolution was 40 meV at 13 eV photon excitation. We show unsmoothed fluorescence spectra in all figures. A high resolution VUV absorption spectrum of acetone was used for calibration of the observed FEX spectral wavelengths.

Mass spectra of acetic acid were measured using a quadrupole mass spectrometer (Leybold Q200) at BESSY I for ions produced by excitation with 20 eV photons, and ion yield curves were obtained through photon energy scans with measuring intervals of 30 meV (as compared with the 150–250 meV intervals in the TEPEPICO measurements of Zha et al. [5]). The yield curves of the principal ions observed are presented in Fig. 3. Ion appearance energies were determined with the aid of semi-log plots of the ion yield curves. The fluorescence and mass spectral measurement techniques used at BESSY I are essentially the same as those used previously for a study of formic acid [10]. Mass spectra of acetic acid were also measured at 25 and 100 eV photon excitation energy at LURE-Orsay, with a reflectron-type time-of-flight mass spectrometer, using a set-up described in detail elsewhere [11,12]. Commercial acetic acid of highest available purity was used without further purification. We note that eventual contamination with water can easily be revealed during the experiments by observing the well-known fluorescence excitation spectrum of OH ($A^2\Sigma^+ \rightarrow X^2\Pi$) emission, which is known to follow VUV photoexcitation of H_2O between 140 and 100 nm [13].

3. Absorption spectroscopy of CH_3COOH

Before discussing the results of our VUV photophysical study of acetic acid it is useful to briefly consider the absorption spectroscopy of this molecule (Fig. 2(c)), which is discussed in more detail elsewhere [9]. Acetic acid has an effective symmetry C_s. The lowest lying excited electronic

state is $1^1A''$, to which photoabsorption from the $1^1A'$ ground state has experimentally been observed as a broad band at about 6 eV, with a very small cross section. It has been attributed to a $\pi^* \leftarrow n_o$ transition [9]. The photodissociation dynamics of the $1^1A''$ state have been studied in detail using laser induced fluorescence spectroscopy, mainly by the group of Guest [14–16]. Decomposition occurs into CH_3CO and OH at 5.69 eV, and secondary decomposition of CH_3CO, probably into CH_3 and CO, is observed at 6.2 eV. It is of interest that the weakest bond in the ground state parent molecule, the C–C single bond, is not broken.

In the VUV regime, below the first ionization energy (10.58 eV, see Section 4.2.2), additional valence transitions as well as Rydberg series converging to the first I.E. have been identified in the absorption spectrum of CH_3COOH [9]. Their absorption cross sections are large as compared to the UV absorption populating the $1^1A''$ state. Above the first ionization energy, we observe increasing photoabsorption until a plateau of about 72 MB is reached at about 17 eV (see Fig. 2(c)). Broad bands in the 12–20 eV region are superimposed on a continuous absorption background. The valence and Rydberg absorption bands of acetic acid have been assigned recently [9]. The VUV photofragmentation behaviour will be discussed in Sections 4.1 (fragment fluorescence) and 4.2 (dissociative ionization).

4. Results and discussion

4.1. Fluorescence observations of fragmentation processes

4.1.1. OH emission

Fig. 1(a) shows the dispersed fluorescence spectrum of acetic acid at an excitation energy of $E_{exc} = 13$ eV (spectral resolution ≈8 nm). The intensity is scaled linearly. At this excitation energy we observe two bands, being respectively the OH ($A^2\Sigma^+ \rightarrow X^2\Pi$) emissions at 308 nm (0–0) and 282 nm (1–0). Suto et al. [3] found no fluorescence in total fluorescence excitation experiments over the excitation range $E_{exc} = 4.9 - 11.7$ eV. They estimated an upper limit of 0.02% for the fluorescence quantum yield. In contrast, Vinogradov and Vilesov [17] observed a significant OH fluorescence quantum yield at wavelengths shorter than 125 nm (9.92 eV), with the yield at 106 nm ($E_{exc} = 11.7$ eV) reported to be 0.2% and at 90 nm ($E_{exc} = 13.78$ eV) to be 0.7%. Our FEX spectrum of OH emission shows that there is very weak fluorescence of this radical at 10 eV (see below).

In Fig. 2(a), we show the fluorescence excitation (FEX) spectrum of the OH $A^2\Sigma^+ \rightarrow {}^2\Pi$ emission ($\lambda_{obs} = 310$ nm) in the 8–22 eV excitation energy range. For comparison, we also show the photoabsorption spectrum of acetic acid (Fig. 2(c)) taken from Leach et al. [9]. In this energy region, our measured relative intensities of the OH FEX bands are normalized, and are situated quantitatively with respect to the fluorescence yield measurements of Vinogradov and Vilesov [17]. We remark that water impurity is negligible in the FEX experiments. This is illustrated by our FEX

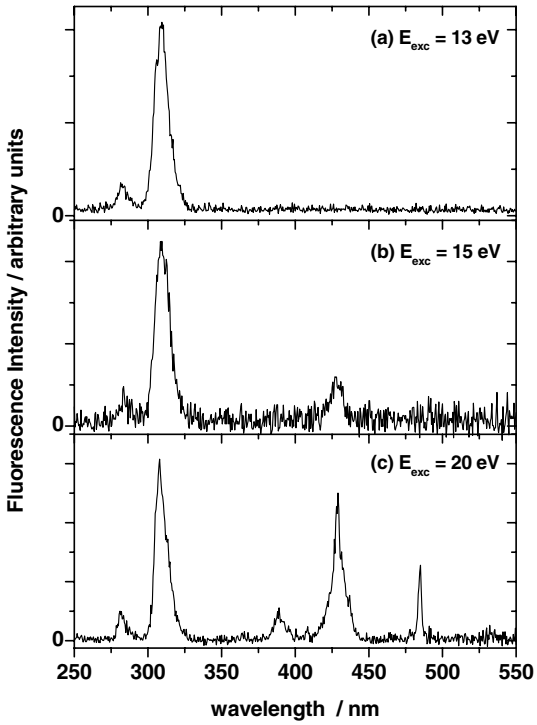

Fig. 1. Dispersed fluorescence spectra observed upon photoexcitation of acetic acid at: (a) $E_{exc} = 13$ eV. Spectral resolution is ≈8 nm. (b) $E_{exc} = 15$ eV. Spectral resolution is ≈8 nm. (c) $E_{exc} = 20$ eV. Spectral resolution is ≈4 nm.

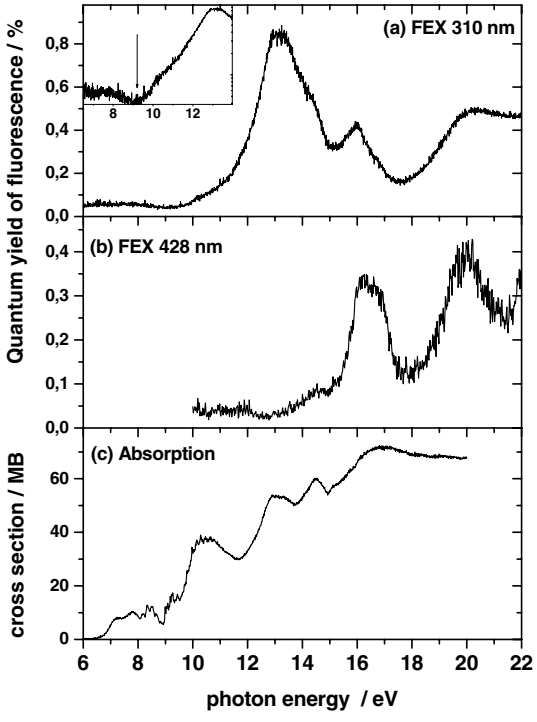

Fig. 2. Fluorescence excitation (FEX) spectra of acetic acid in the 6–22 eV photon excitation region: (a) OH (A-X) ($\lambda_{obs} = 310$ nm), semi-log plot of the signal shown as an insert; (b) CH (A-X) ($\lambda_{obs} = 428$ nm) emissions; (c) Photoabsorption spectrum of acetic acid in the 6–20 eV region [9].

spectrum of OH emission detected at 310 nm, in which the detailed structure, in particular between 10 and 12.4 eV, of the known OH emission in the FEX spectrum of water [12] is virtually absent. We note also that the fluorescence quantum yield of water (OH emission) in this region is at least 10 times greater than our measured yield of 310 nm emission [12].

Our onset for the 310 nm band is at 9.2 ± 0.1 eV as determined from a semi-log plot of the signal, shown as an insert in the threshold region of the OH (A) FEX spectrum in Fig. 2(a). The onset reported by Vinogradov and Vilesov [17] is 9.36 ± 0.04 eV. Their yield curve extends to the maximum fluorescence quantum yield of 0.7% at 13.78 eV. Our OH fluorescence yield curve extends to $E_{exc} =$ 22 eV and is very similar in profile to that of Vinogradov and Vilesov over the 8–13.77 eV excitation range common to both studies, but our maximum quantum yield is found at 13.3 eV. We note that our onset energy coincides with some of the lowest energy Rydberg bands converging to the ion ground state in the absorption spectrum [9], whereas the region of the maximum OH fluorescence yield is that of broad overlapping Rydberg bands converging to the second electronic excited state of the acetic acid ion [9]. A second, less intense, OH fluorescence yield maximum is observed at 15.8 eV, followed by a further rise to the 20 eV region. Using the OH fluorescence quantum yields of Vinogradov and Vilesov [17] to calibrate our own values, we calculate that the quantum yield of fluorescence is 0.9% for OH (A) emission at $E_{exc} = 13.3$ eV, 0.4% at $E_{exc} =$ 16 eV and 0.5% at $E_{exc} = 20$ eV. Although our experiments do not allow us to observe neutral fragments in their electronic ground states, on energy grounds it is reasonable to assume that the processes leading to the observed fluorescence are in competition with acetic acid dissociation processes giving non-excited products. The latter processes would constitute more efficient relaxation pathways of the electronic excited states of the parent molecule.

From enthalpy of formation (ΔH_f) data (Table 1) and the OH ($A^2\Sigma^+ - X^2\Pi$) T_0 value (4.017 eV [25]), we calculate the thermochemical onset to be 8.79 eV for the reaction

$$CH_3COOH \rightarrow CH_3CO + OH\ (A^{2+}) \quad (1)$$

This is 400 ± 100 meV below our measured onset energy of the OH (A) emission. The difference between the thermochemical and the measured onset energy could indicate the existence of a potential barrier between the CH_3COOH excited state and the dissociation surface leading to the OH (A) fragment. If this were the case, one would predict that the initial rise of the OH emission yield beyond the onset would be slow, which is not incompatible with our measured yield curve (Fig. 2(a)). The difference between the thermochemical and the measured onset energies probably also reflects the fact that the detection sensitivity for fluorescence photons is limited, so that our measured onset energy is an upper limit.

We note, however, that since the reaction $CH_3COOH \rightarrow CH_3CO + OH$ ($X^2\Pi$) has an observed onset at 5.69 eV [15], one might expect the appearance energy for reaction (1) to be 9.707 eV, well above our observed and the thermochemical onset energies. Hunnicutt et al. [15] have shown that the reaction forming OH ($X^2\Pi$) involves a potential barrier of the order of 610 meV. From this, and our AE $= 9.2 \pm 0.1$ eV for OH ($A^2\Sigma^+$) emission we infer that dissociation to the excited OH radical, via Rydberg state excitation at 9 eV, occurs without a potential energy barrier.

At higher energies, we observe a OH FEX maximum at about 13.3 eV, which can be correlated with the absorption feature at about 13–13.3 eV [9], as mentioned above, and an EELS peak at 13 eV [26]. The fall-off after this maximum occurs in a region where there is a rise of CH emission (see below). There are less intense OH FEX peaks at about 15.8 eV, perhaps related to the absorption inflexion at 15.77 eV, and at about 20 eV. An inflexion at about 14.5 eV may be related to the absorption peak at 14.5 eV. There is also a peak at 14.5 eV in the CH emission FEX spectrum (see later). We note that since the our AE of CH_3CO^+ is 11.60 ± 0.05 eV (Section 4.2.3), and the excited OH(A) state energy is 4.017 eV [25], we can expect the opening of the dissociative ionization channel

$$CH_3COOH \rightarrow CH_3CO^+ + OH\ (A^{2+}) \quad (2)$$

to be at 15.69 eV, i.e., not far from the beginning of the rise in the OH emission yield at 15.2 eV. The fall-off from 16 eV parallels the disappearance, in TPEPICO experiments, of the CH_3CO^+ ion in this energy region [5]. The OH fluorescence yield curve rises again at 17.9 eV. We considered whether this could be due to opening of the channel

$$CH_3COOH \rightarrow CH_3^+ + OH\ (A^{2+}) + CO \quad (3)$$

but the thermochemical limit for this channel, 19.24 eV, is over 1 eV above the rise point.

4.1.2. CH and H emissions

As excitation energy increases beyond 13 eV in our dispersed fluorescence measurements, we see not only the OH emission bands, but also at and above $E_{exc} = 15$ eV (Fig. 1(b), spectral resolution ≈8 nm), the (0,0) band of the CH ($A^2\Delta \rightarrow X^2\Pi$), transition (Q head 431.4 nm). In addition, we observe extremely weakly the (0,0) band of the CH ($B^2\Sigma^- \rightarrow X^2\Pi$) transition at 388 nm. This is reinforced at $E_{exc} = 20$ eV (Fig. 1(c), resolution 4 nm) where, in addition we observe the Hβ line at 486.1 nm and the Hδ line at 410.1 nm.

We note that the emission band at 431 nm has a broad base (Fig. 1(c)) so that it is necessary to investigate whether it has more than one component. A possible extra component would be H-Balmer-γ ($n = 5 \rightarrow 2$) emission at 434 nm. H-Balmer-γ could result from the dissociation process:

$$CH_3COOH \rightarrow CH_3COO + H\ (n = 5) \quad (4)$$

which has a thermodynamic onset energy of 17.55 eV. However, this thermochemical value is much higher than

the observed onset energy for the 431 nm emission which is AE = 12.8 ± 0.1 eV as discussed below. We conclude by assigning the 431 nm band to CH (A) emission, but do not exclude a contribution of H-Balmer-γ (5–2) at excitation energies above 17.5 eV. We note that from our FEX spectrum (Fig. 2(b)) the fluorescence quantum yield for CH (A-X) is 0.35% at 16 eV and 0.4% at 20 eV but with a minimum of about 0.12% at 17.8 eV, a region where there is a minimum in the OH emission yield, and a further minimum at about 21.3 eV. The increase in the 428 nm FEX signal between 17.8 and 20 eV might be due, in part to H-Balmer-γ (5–2) emission, as mentioned above.

We next discuss the fluorescence band at 485 nm (Fig. 1(c)), whose observed small bandwidth of 4 nm, (we mention that 4 nm was our resolution limit in the 20 eV excitation dispersed fluorescence measurements), suggests that it is due to an atomic emitter. The wavelength of H-Balmer-β emission is 486.1 nm so that, at our spectral resolution, this is the most probable assignment. Its thermochemical onset energy is calculated to be 17.25 eV. Another possible assignment is to the (0,1) band of the $A^2\Delta \rightarrow X^2\Pi$ transition of the CH radical whose Q head should occur at 489 nm. We did not measure the FEX spectrum of the 485 nm band, so we cannot affirm the respective importance of these two possible emitters as a function of excitation energy. However, in the set of the dispersed fluorescence spectra, the 485 nm band is observed at 20 eV but not at lower excitation energies so, on thermochemical grounds, it is most probably due to H-Balmer-β emission.

In Fig. 2(b), we show the fluorescence excitation (FEX) spectrum of the CH emission ($\lambda_{obs} = 428$ nm) in the 8–22 eV excitation energy range. Our measured relative intensities of the CH FEX bands are normalized as discussed above for the OH emissions. Our observed onset for 428 nm emission of CH (A-X) is at $E_{exc} = 12.8 \pm 0.1$ eV. This AE might correspond to the threshold energy of the reaction

$$CH_3COOH \rightarrow CH_3OO + CH\,(A) \quad (5)$$

The calculated thermochemical threshold energy is 13.74 eV. However, the unknown nature of the structure of the CH_3OO radical that would be formed by photodissociation of acetic acid prevents us from validating this calculated thermochemical threshold energy. At higher energies there is a minor FEX peak at about 14.5 eV, mentioned above, and a second onset occurs in the yield curve at 14.9 eV, consistent with the reaction

$$CH_3COOH \rightarrow CH\,(A) + CH_3 + O_2 \quad (6)$$

calculated to have a thermochemical threshold energy of 15.05 eV. Major peaks occur at 16.2 eV (absorption peak at 16.83 eV) and at about 20 eV. Since the FEX and absorption bands are broad in this energy region we cannot say whether OH (A) and CH (A) stem from different or common CH_3COOH superexcited states.

4.1.3. Absence of oxyl radical emissions

It is of interest that no emission of the HCOO radical was observed over the 10–20 eV excitation energy range, in contrast to the case of formic acid excitation, in which this radical emits a series of close-lying bands between 335 and 480 nm [10]. In formic acid, FEX experiments show that the formyloxyl radical HCOO emission is excited only between 9 and 13 eV. In acetic acid, we did not study dispersed fluorescence below 10 eV photon excitation. The excited HCOO radical would be formed in acetic acid by $CH_3COOH \rightarrow CH_3 + HCOO^*$. The thermochemical limit for this process is 8.89 eV, so that it would be worth exploring the excitation range 8–10 eV.

One must also consider the H-loss process analogous to formic acid, i.e., $CH_3COOH \rightarrow CH_3COO^* + H$. The acetyloxyl radical CH_3COO emission spectrum is not known. In fact, CH_3COO has not been detected spectroscopically due to its strong tendency to decarboxylate [3,27–29]. Peyerimhoff et al. [28] calculate that for a particular CH_3COO structure, its lowest state is $^2A''(^2B_2)$, above which lie $^2A'(^2A_1)$, nearly degenerate with an excited $^2A''(^2B_2)$ electronic state at 1.98 eV. Easy dissociation of CH_3COO to $CH_3 + CO_2$ is suggested. The calculations of Rauk et al. [29] give 4 local minima structures for the ground state of CH_3COO. Facile dissociation to $CH_3 + CO_2$ is also predicted for excited states. Thus, CH_3COO formed in an excited state would dissociate rather than emit, in contrast to HCOO*.

4.2. Dissociative ionization

4.2.1. Initial survey of mass spectra

The mass spectra of acetic acid excited by 20, 25 and 100 eV photons are reported in Table 2. The relative intensities of the m/z peaks are normalized to that of $m/z = 43$. The same mass peaks are observed at 20 and 25 eV excitation with few important changes in relative intensities, in spite of the fact that different mass spectrometers were used in these two cases. In the quadrupole mass spectrometer used at 20 eV excitation, the relative ion peak intensities are not proportional to abundances because ion detectivity and resolution are a function of ion mass.

One of the intensity changes concerns the parent ion, which increases in relative intensity, with respect to $m/z = 43$, with increasing excitation energy. This appears to be due to a fall-off in the yield of $m/z = 43$ as increased fragmentation occurs with increasing E_{exc}, so that the relative yield of the fragment ion $m/z = 43$ to that of the parent ion $m/z = 60$ decreases with increasing E_{exc}, as confirmed in the region up to 25 eV by a direct comparison between the PIMS ion yield curves of $m/z = 60$ and $m/z = 43$, measured with the same quadrupole mass spectrometer at BESSY I.

The breakdown curves of the TPEPICO study of Zha et al. [5] show that the parent ion is formed only between the IE and 11.5 eV. Therefore, another level of explanation of the behaviour of the $m/z = 60$ relative yield is that with

Table 2
Mass spectra of acetic acid. Relative intensities at 20, 25 and 100 eV photon excitation energies

m/z	20 eV photons	25 eV photons	100 eV photons	Assignment
61	<1	2	4	CH_3COOH^+ (^{13}C)[a]
60	19	29	53	CH_3COOH^+
46	1.5	3	6	$HCOOH^+$
45	80	79	84	$COOH^+$
44	2	7	14	CO_2^+
43	100	100	100	CH_3CO^+
42	11	13	24	CH_2CO^+
41	0.5	2	10	C_2HO^+
40	0.2	0.5	4	C_2O^+
32	3	5	12	O_2^+; CH_3OH^+
31	7	11	13	CH_2OH^+
30		1	2	H_2CO^+
29	7	18	50	HCO^+
28	9	8	38	CO^+
27			0.5	$C_2H_3^+$
26			4	$C_2H_2^+$
25			6	C_2H^+
24			4	C_2^+
18	16	61	182	H_2O^+
17	8	27	74	OH^+
16	13	11	40	CH_4^+
15	83	78	106	CH_3^+
14	6	11	64	CH_2^+
13	1	12	37	CH^+
12	0.5	0.2	20	C^+
2		0.3	5	H_2^+
1		32	219	H^+

[a] See text.

increasing E_{exc}, there is a relative increase in energy deposition to the 13a′ orbital ($E_{vert} = 10.84$ eV) of acetic acid, which is the expected behaviour for a non-bonding MO [9] and which is confirmed by a comparison between He I and He II PES of acetic acid [30].

Both types of explanation are probably relevant when we go to the mass spectrum obtained with $E_{exc} = 100$ eV, measured with the same mass spectrometer as that used at 25 eV, since in this case, the ratio of the parent ion intensity to that of the sum of the fragment ions is very similar to that at $E_{exc} = 25$ eV. This is consistent with the fact that only two of the 12 valence shell molecular orbital excitations lie at energies above 25 eV, i.e., the 6a′ and 5a′ M.O.s calculated to lie at 30.91 and 33.34 eV, respectively [9]. We note that the fragmentation pattern at 100 eV photon excitation includes the $m/z = 24$–27 ions which are absent at $E_{exc} = 25$ eV. We have assigned them respectively to C_2^+, C_2 H^+, $C_2H_2^+$ and $C_2H_3^+$. These monocations could have resulted from Coulomb dissociation of dications that can be formed at $E_{exc} = 100$ eV, but this remains to be verified.

Other ions whose intensities change significantly in going from $E_{exc} = 20$ to $E_{exc} = 25$ eV and then to $E_{exc} = 100$ eV include $m/z = 29$ (HCO^+) and $m/z = 18$. The latter ion is assigned to H_2O^+, which may, in part, be due to a water impurity. The ratio of $m/z = 17$ (OH^+) to $m/z = 18$ (H_2 O^+) is 0.5 at $E_{exc} = 20$, whereas if the $m/z = 18$ was exclusively from a water impurity, the expected ratio at $E_{exc} = 20$ eV would be 0.3 [31].

The fragment ions $m/z = 14$ and $m/z = 13$ increase considerably in intensity with increase in E_{exc}. This corresponds to increasing ability to lose a hydrogen atom, culminating in the appearance of $m/z = 12$ (C^+), in the processes forming the hydrocarbon series CH_3^+, CH_2^+, CH^+, C^+. We note that an electron impact study on acetic acid gave the appearance energy of the C^+ ion to be 22.5 ± 0.5 eV [32].

We now discuss in further detail the ions observed by mass spectrometry.

4.2.2. Parent ion

The $m/z = 61$ ion is assigned to CH_3COOH^+ containing one ^{13}C atom. Its intensity in the LURE experiments at 25 and 100 eV photon excitation energy, is two or three times greater than that expected with respect to the ^{12}C parent ion. The $m/z = 61$ ion may therefore have a small contribution from an $(M + 1)^+$ ion. The latter can be formed by rapid fragmentation of acetic acid dimer cations, if these are present, or it might result from a complex with a water impurity. The $(M + 1)^+$ ion is indeed the dominant ion in the mass spectrum of the acetic acid dimer [33]. A test for the $(M + 1)^+$ ion resulting from fragmentation of a dimer cation would be its 200 meV smaller appearance potential with respect to the ^{13}C monomer ion [33]. Unfortunately, the $m/z = 61$ ion was too weak for an appearance energy measurement.

The CH_3COOH^+ parent ion, at $m/z = 60$, has an ionization energy IE = 10.58 ± 0.02 eV from our ion yield measurements (Fig. 3(a)). This value is lower than those obtained by other PIMS measurements, IE = 10.644 ± 0.002 eV [34]; 10.66 ± 0.01 eV [4]; 10.64 ± 0.05 eV [33].

Our parent ion yield curve shows inflexions and structures, and has a maximum intensity at ≈17.2 eV. A direct comparison of the $m/z = 60$ ion yield curve (Fig. 4(d)) with the absorption spectrum (Fig. 4(a)) and the photoelectron spectrum (Fig. 4(b)) of acetic acid showed several correspondences. The first PES band has a main peak at 10.84 eV and two side features. These are seen as inflexions on the parent ion yield curve. The ion yield features in the 11.6 and 12.7 eV regions, correlate with minima in the photoelectron spectrum but have no evident correspondence in the absorption spectrum. The maximum at 14.5 eV correlates with features in the photoelectron and absorption spectra whose energies correspond to the formation of the $2^2A'$ and $3^2A'$ electronic states of the acetic acid cation [9]. The dips in the ion yield curve at 14.9 and 15.8 eV appear to be real since they were observed only on the parent ion yield curve and are observed also in the absorption spectrum. However, the integrated HeI and He II (Fig. 4(c)) photoelectron spectra [35], which mirror to a certain extent the parent (and also some fragment) ion yield curves, show no dips at 14.0 and 15.8 eV. In general, the integrated HeI and HeII PES spectra, given up to 19 eV by Carnovale et al. [35], but which tend to flatten out

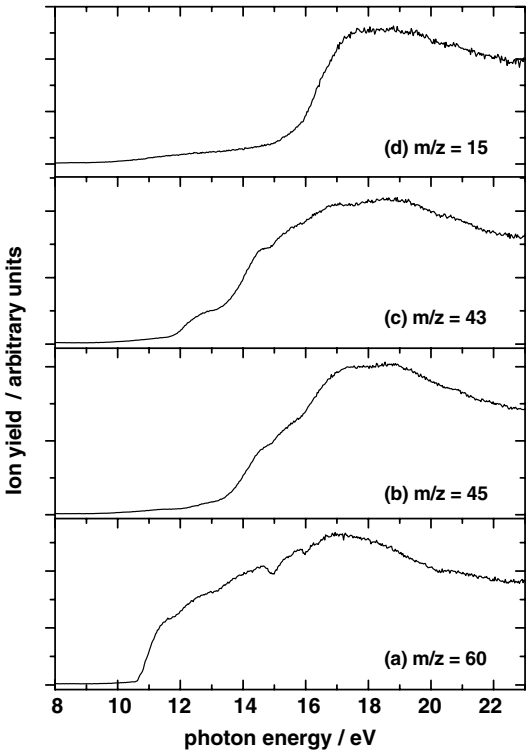

Fig. 3. Photoion yield curves: (a) $m/z = 60$ (CH_3COOH^+); (b) $m/z = 45$ ($HOCO^+$); (c) $m/z = 43$ (CH_3CO^+); (d) $m/z = 15$ (CH_3^+).

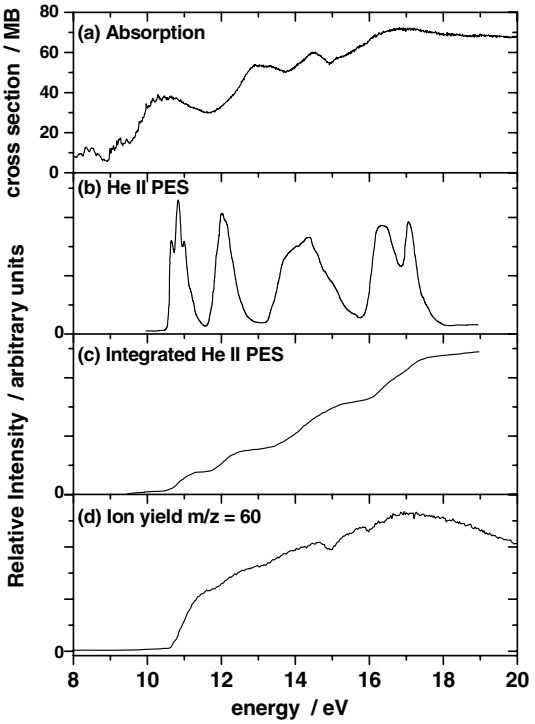

Fig. 4. Acetic acid: (a) photoabsorption spectrum [9]; (b) HeII photoelectron spectrum [35]; (c) integrated HeII photoelectron spectrum [35]; (d) CH_3COOH^+ ion yield curve.

beyond 17 eV, have large steps corresponding to opening up of newly accessed electronic states of the ion. These steps are indeed mirrored, in attenuated fashion, in the parent ion yield curve. We remark that the photoelectron spectra do not contain features resulting from autoionising processes, which could only be expected close to the excitation energy, whereas the ion yield curves result from both direct ionization and autoionization processes. The latter are implicitly contained, in proportion to ionization yields, in the absorption spectra.

4.2.3. Fragment ions

We note the virtual absence of a peak at $m/z = 59$. An ion of this m/z would be CH_3COO^+, formed by loss of a hydrogen atom from the hydroxyl group of the parent ion,

$$CH_3COOH^+ \rightarrow CH_3COO^+ + H \quad (7)$$

or CH_2COOH^+ formed by loss of a hydrogen atom from the methyl group,

$$CH_3COOH^+ \rightarrow CH_2COOH^+ + H \quad (8)$$

In formic acid, the hydrogen atom loss reaction is from the CH group, to form $COOH^+$ and not from the hydroxyl group to form $HCOO^+$ [36]. In acetic acid the analogous reaction to that occurring in formic acid is rupture of the C–C bond, to form the very intense fragment ion $COOH^+$ ($m/z = 45$) by loss of a methyl group. We note that KER modelling by Zha et al. [5] indicated that the KER in $COOH^+$ formation is non-statistical; it appears to arise mainly from the excess internal energy of the activated complex and implies that the reverse activation energy is negligible.

The $m/z = 45$ ion is assigned to $COOH^+$ (=$HOCO^+$ [37]). Its yield curve (Fig. 3(b)) has an AE = 11.7 ± 0.05 eV. The TPEPICO measurement value is 11.53 ± 0.10 eV [5]. Other reported AEs are the PIMS value 11.90 ± 0.03 eV [4] and, from electron impact studies, AE = 12.9 ± 0.1 eV [38] and 12.27 ± 0.05 eV [39]. The thermochemical onset energy for the reaction

$$CH_3COOH \rightarrow CH_3 + COOH^+ \quad (9)$$

is calculated to be 12.18 eV, but this suffers from the fact that the heat of formation of $COOH^+$ used in the calculation is for an unspecified ion structure of the ion.

We note that there is some structure in the $m/z = 45$ ion yield curve (Fig. 3(b)), in particular knees at 14.5 eV, i.e., where CH_3^+ becomes very noticeable (see below) and close to a dip in the parent ion yield curve. The steps in the integrated HeI and HeII PES spectra [35] (Fig. 4(c)) are weakly mirrored in the $m/z = 45$ ion yield curve. The integrated PES curves tend to flatten out after 17 eV, as does the this ion yield curve, which forms a plateau 17–18.5 eV, after which it drops to 23 eV.

The major ion in the mass spectrum, $m/z = 43$, assigned to CH_3CO^+, is formed by loss of OH from the parent ion. From our ion yield curve we obtain AE = 11.45 ± 0.05 eV for this ion (Fig. 3(c)). This is in good agreement with the TPEPICO AE = 11.37 ± 0.07 eV [5] and a PIMS AE = 11.38 ± 0.08 eV [4]. It is also in good agreement with the PIMS value 11.54 eV of Traeger et al. [40] and the

electron impact values 11.54 ± 0.05 eV [41] and 11.4 ± 0.15 eV [38]. An early electron impact study gives a higher value, 11.75 eV [39], but the uncertainty in this measurement was not reported. The calculated thermochemical onset value, 11.67 eV, is higher than other experimental values mentioned above, except for the electron impact value 11.75 eV of Haney and Franklin [39]. The thermochemical value probably reflects the unknown uncertainty in the adiabatic ionization energy of CH_3CO, whose value is reported to be 7.21 ± 0.05 eV [42]. The above discussion suggests that its true value is lower, possibly of the order of 6.6–6.8 eV. One can indeed question whether the heat of formation and the ionization energy of the acetyl radical are sufficiently well known and whether the structure of the CH_3CO radical in previous determinations of the heat of formation [20,43,44] was indeed the acetyl radical.

From their KER study Zha et al. [5] suggested that the formation of CH_3CO^+ does not result from a simple cleavage reaction, and that it involves an energy barrier and probably proceeds via an intermediate. The reasonably good agreement between our measured AE and the calculated thermochemical AE for this ion does not support these suggestions. We note that from their determination of the heat of formation of the CH_3CO^+ ion, by a PIMS study of a series of substituted methyl ketones, Traeger et al. [40] concluded that KER measurements made at energies greater than threshold cannot be applied straightforwardly as thermochemical corrections for the experimental CH_3CO^+ AEs. Following their electron impact dissociative ionization measurements, Holmes and Lossing [41] also consider that loss of OH occurs at the thermochemical threshold for production of CH_3CO^+. We remark that it is possible that in the experiments of Zha et al. [5], there occurred some interconversion to the enol form of acetic acid [45,46]. It is of interest that from the rate constants for CH_3 and OH loss as a function of internal energy in the CH_3COOH^+ ion, calculated by McAdoo et al. [46], one would expect AE ($m/z = 45$) − AE ($m/z = 43$) ≈ 750 meV, whereas we observe a much smaller difference, of about 250 meV, which agrees reasonably well with the results of the rate constant calculations of Zha et al. [5].

There is some marked structure in the $m/z = 43$ ion yield curve, in particular knees at 12.7 and 14.5 eV. The integrated HeI and HeII PES spectra [35] (Fig. 4(c)) have large steps corresponding to opening up of newly accessed electronic states of the ion. These steps are mirrored in the $m/z = 43$ ion yield curve (Fig. 3(c)), which has a quasi plateau 17–19.3 eV, with a maximum at about 19 eV, after which it drops to 23 eV. The integrated curve (Fig. 4(c)) tends to flatten out after 17 eV.

The weak $m/z = 46$ and 44 ions are assigned to $HCOOH^+$ (loss of CH_2) and CO_2^+, respectively. An alternative assignment for $m/z = 44$ would be the CH_3COH^+ ion. However, in this case the neutral loss species is an oxygen atom but this would mean rupture of a C=O bond, which is unlikely. Furthermore, reaction (10),

$$CH_3COOH^+ \rightarrow CH_4{}^+ + CO_2 \quad (10)$$

the charge switch of the reaction $CH_3COOH^+ \rightarrow CH_4 + CO_2^+$, certainly occurs (see below). The CO_2^+ reaction would be less favoured, from the the Stevenson-Audier-Harrison (SAH) rule concerning the dissociation of odd electron ions [37], since CO_2 has a higher IE (13.77 eV) than CH_4 (12.51 eV) [18]. The relative intensities of the $m/z = 44$ and $m/z = 16$ ions (Table 2) are consistent with this interpretation. The calculated thermochemical appearance energy of CO_2^+ is 13.4 eV.

Formation of the minor ion $m/z = 42$, assigned to CH_2CO^+, involves the loss of H_2O from the parent ion:

$$CH_3COOH^+ \rightarrow CH_2CO^+ + H_2O \quad (11)$$

This may involve a complicated reaction and two possible pathways have been proposed [41,45]. The low intensity suggests that H_2O loss is much less favoured than the competing OH loss reaction, despite having a lower thermochemical threshold. We note that at 20 eV excitation the ratio of intensities of the $m/z = 43$ to the $m/z = 42$ peaks (loss of OH cf. loss of H_2O) is 9.1 and that this is very similar to the ratio 11.5 observed in metastable transitions measured by the MIKES technique [45]. Holmes and Lossing [41] state that elimination of H_2O involves a 1,3 hydrogen shift, proceeding via a H transfer from CH_3 to hydroxyl OH and mention that the AE is difficult to measure. Villem and Akopyan [4] report a PIMS AE = 10.8 ± 0.1 eV for the $m/z = 42$ ion, which is close to the 11.09 eV calculated thermochemical threshold.

The $m/z = 32$ minor ion could be O_2^+ or CH_3OH^+. These possible assignments involve loss of C_2H_4 and CO, respectively, from the parent ion. Isotopic studies are required to pin down the assignment. The $m/z = 31$ minor ion can be assigned to CH_3O^+ or CH_2OH^+, involving the loss of the HCO radical (reactions (12) and (13), respectively).

$$CH_3COOH^+ \rightarrow CH_3O^+ + HCO \quad (12)$$

$$CH_3COOH^+ \rightarrow CH_2OH^+ + HCO \quad (13)$$

Zha et al. [5] have shown that the $m/z = 31$ ion is the hydroxymethyl cation CH_2OH^+. Our calculated thermochemical onsets 13.64 eV (CH_3O^+) and 12.26 eV (CH_2OH^+) are much lower than the observed AE = 14.99 ± 0.12 eV reported by Zha et al. [5]. However, Selim and Helal [47] observed an electron impact value AE = 12.05 ± 0.1 eV, and assigned this ion to CH_2OH^+. This AE is compatible with our calculated thermochemical AE for CH_2OH. We remark that formation of both CH_3O^+ and CH_2OH^+ should involve atomic rearrangements. Zha et al. [5], by deuteration, show that the two oxygen atoms become equivalent for formation of $m/z = 31$ and also concluded that this ion is likely to be CH_2OH^+. The process may involve a two-step rearrangement prior to fragmentation, going through the enol ion stage.

In principle, the $m/z = 29$ ion could be assigned to either HCO^+ or COH^+, formed by loss of CH_3O from the parent ion. However, the absence of a $m/z = 30$ peak in the mass spectrum of CH_3COOD indicates that the $m/z = 29$ ion in the CH_3COOH dissociative ionization is HCO^+ and not COH^+[5]. It is a minor ion at $E_{exc} = 20$ eV but increases considerably in relative intensity at higher excitation energies. Two formation pathways were considered by Zha et al. [5]:

$$\text{(i)}\ CH_3COOH^+ \rightarrow CH_2OH^+ + COH \rightarrow HCO^+ + COH + H_2 \quad (14)$$

$$\text{(ii)}\ CH_3COOH^+ \rightarrow COOH^+ + CH_3 \rightarrow COH^+ + CH_3 + O \quad (15)$$

We envisage a third dissociation channel:

$$\text{(iii)}\ CH_3COOH^+ \rightarrow COH^+ + CH_3O \quad (16)$$

The thermochemical appearance energies for reactions (14)–(16) were calculated, considering both HCO and COH isomers as neutral products in reaction (14), and both CH_3O and CH_2OH isomers in reaction (16). This gave five thermochemical AE values: 12.86 and 13.48 eV for reaction (14), 17.13 eV for reaction (15) and 12.84 and 13.22 eV for reaction (16). The observed AE = 15.91 ± 0.13 eV in the TPEPICO experiments [5], eliminates reaction (15). Reaction (16) is a charge switch reaction to formation of the $m/z = 31$ ion (reactions (12) and (13)). The IE of HCO is 8.10 ± 0.05 eV [19], whereas CH_2OH has an IE of 7.56 ± 0.01 eV [19]. These values are not very different which makes it reasonable that the $m/z = 29$ and 31 ions are observed with similar intensities at $E_{exc} = 20$ eV but, as mentioned above, $m/z = 29$ increases considerably in relative intensity at 25 and 100 eV.

The $m/z = 28$ ion, assigned to CO^+ is weak at 20 and 25 eV excitation energies but quite intense at $E_{exc} = 100$ eV (Table 2). The neutral loss species is CH_3OH.

$$CH_3COOH^+ \rightarrow CO^+ + CH_3OH \quad (17)$$

The alternative assignment of $m/z = 28$ is $C_2H_4^+$, formed by loss of O_2 from the parent ion, can be rejected since its calculated thermochemical AE = 15.53 eV is greater than the observed AE = 15.3 ± 0.1 eV [38], which is close to our calculated thermochemical AE = 15.27 eV for reaction (17).

The $m/z = 16$ ion is assigned to CH_4^+, formed by loss of CO_2 from the parent ion,

$$CH_3COOH^+ \rightarrow CH_4^+ + CO_2 \quad (18)$$

This assignment is in agreement with those of Zha et al. [5], who observe an AE = 12.31 eV, and by Villem and Akopyan [4], who report 12.1 ± 0.1 eV, values which agree well with our calculated thermochemical AE = 12.13 eV.

The very important $m/z = 15$ ion is assigned to CH_3^+, formed by loss of COOH from the parent ion. Two different formation processes have been suggested [5]:

$$\text{(i)}\ CH_3COOH^+ \rightarrow CH_3^+ + COOH \quad (19)$$

$$\text{(ii)}\ CH_3COOH^+ \rightarrow CH_3CO^+ + OH \rightarrow CH_3^+ + CO + OH \quad (20)$$

The calculated thermochemical appearance energies of CH_3^+ are 13.51 eV (reaction (19)) and 15.08 eV (reaction (20)). Our measured AE(CH_3^+) = 14.28 ± 0.10eV (Fig. 3d), which is smaller than the TPEPICO measured AE = 14.73 ± 0.15 eV [5], but similar to the electron impact AE = 14.0 ± 0.15 eV [39], appears to favour reaction (19), which corresponds to the charge switch of reaction (9) forming $COOH^+$. The electron impact value AE = 16.08 eV of Hirota et al. [48] is certainly erroneous. The difference of about 800 meV between the thermochemical onset energy for reaction (19) and the observed AE of CH_3^+ suggests that the dissociation process involves a potential barrier. We note that the analogous neutral photochemical reaction has a very low probability [15].

The appearance energy results suggest that reaction (19) is operative in the threshold region. Since IE(CH_3) = 9.84 ± 0.01 eV and IE(COOH) ⩽ 8.19 eV [49], the SAH rule [37] certainly favours reaction (19) in this excitation energy region. However, Zha et al. [5] argue in favour of reaction (20), presumably at higher energies, on the basis that the breakdown graph suggests that CH_3^+ increases simultaneously with a decrease in CH_3CO^+. In fact the CH_3^+ signal increases to become similar with the CH_3CO^+ yield in TPEPICO measurements at about 17 eV [5]. We note that the $m/z = 15$ ion yield curve has a quasi-plateau 17.5–19.5 eV, very similar to that of the $m/z = 45$ ion and where the integrated PES curve [35] tends to flatness.

5. Astrophysical implications

The results of our study are relevant to astrophysics in three areas: the interstellar medium (ISM), comets and meteorites. It has also some implications for exobiology. Acetic acid is considered to be one of the building blocks of life [50]. If preserved during the formation of the solar nebula, it could be brought to Earth via asteroids, comets and meteorites which can provide protective environments. In HI regions of the interstellar medium (ISM), the upper limit of UV radiation is 13.6 eV. Acetic acid in unscreened regions, subject to VUV radiation below 13.6 eV, will form ions above 10.6 eV. The ionization quantum yield (not yet measured), is unlikely to reach unity until about 17 ± 1 eV [1,51], and in the intervening energy region, superexcited states of acetic acid will be formed, states that relax mainly by dissociation and/or autoionization. At an excitation energy of 13.6 eV, i.e., 3 eV above the ionization limit, an ionization yield of about 50% is likely, as can be predicted on the basis of measurement of ionization quantum yields of polyatomic molecules [1,31,51]. Dissociative ionization will occur at photon excitation energies above 11.6 eV, the threshold for CH_3CO^+ formation. We note that photolysis of acetic acid in argon matrices by irradiation with a

hydrogen lamp ($E_{exc} \leqslant 10.2$ eV) results in the formation of CO_2 [52].

Protection from the destructive effects of VUV radiation is thus necessary in order to achieve detectable amounts of acetic acid in the ISM. Acetic acid has been observed in the ISM in hot molecular cores, which are warm condensations inside molecular clouds associated with active star formation regions, whose density is such that they will offer molecules some protection against radiation. A typical source is the molecular cloud complex Sgr B2, the acetic acid being found in a very small core, about 0.1 pc across [6]. This polyatomic molecule is probably synthesized on dust grain surfaces [53] and ejected into the ISM by evaporation or by shocks. It has been suggested that CH_3CO^+, the principal fragment ion in VUV dissociation of acetic acid, can react with water in the gas phase reaction to form $CH_3COOH_2^+$, followed by dissociative electron recombination to produce CH_3COOH [54]. There are other, more recent, suggestions for gas phase synthesis of acetic acid via ion molecule reactions [55]. Observations toward W51e2 show that the distribution of CH_3COOH is coincident with that of its much more abundant isomer, methyl formate $HCOOCH_3$, thus suggesting a similar formation mechanism [56].

It is known that ammonia and acetic acid can combine, in the laboratory, to produce aminoacids, in particular, glycine [57]. This could possibly occur in the ISM, where glycine has recently been reported in hot molecular cores in three regions of ongoing massive star formation [58]. This process of aminoacid formation is probably more easily achieved in cometary and meteoritic material contexts, which can provide various catalytic media and radiation screening.

Of the ions that we observe by dissociative ionization we note that HCO^+, $HOCO^+$ and CH_2OH^+ have been observed in the ISM, so that acetic acid is a possible parent molecule for part of the observed abundances. The dissociative photoionization of acetic acid to form HCO^+ is energetically possible above 12.85 eV, but its yield would be low in HI regions. The $HOCO^+$ ion is also observed in the galactic centre region and in Sgr B2 [59,60]. Since this is a region of the ISM where CH_3COOH has been observed, $HOCO^+$ could be produced, at least in part, from acetic acid (AE = 11.8 eV). The formation of CH_2OH^+ can occur above 12.05 eV, as discussed above, i.e., within the HI energy region.

Although it has not yet been observed in comets, acetic acid is strongly expected to exist in this medium where, for example in comet Hale-Bopp, its abundance has an upper limit, relative to H_2O, of 0.06%, as compared with 0.09% for formic acid [7]. Comets are thought to be one of the possible sources of extraterrestrial supply of organic material to the early Earth [61]. The species in the comet coma and tail are not screened from solar VUV radiation, so that acetic acid, if present, would be rapidly dissociated. Of the three ions observed by radioastronomy in comet Hale-Bopp two, CO^+ and HCO^+ [62], are species that can be formed by dissociative ionization of acetic acid. In future cometary observations it would be of interest to attempt to observe the ion CH_3CO^+ which would be a good marker of the presence of acetic acid, and also $HOCO^+$, which can be formed from both formic [10] and acetic acids. Observations of OH (A-X) emissions from acetic acid dissociation would require space observatory means but would probably be swamped by OH emission from water photodissociation processes.

Acetic acid is found in many meteorites. It is the most abundant of the monocarboxylic acids in the Murchison meteorite [63]. The work of Huang et al. [63] supports the suggestion of Cronin and Chang [64] that monocarboxylic acids may be mostly unaltered interstellar molecules.

Our results demonstrate that the spectroscopy and photophysics of acetic acid have potential applications in astrophysics and exobiology, in particular for understanding the formation and dissociation processes of this species, as well as properties of its dissociation products.

6. Summary and conclusions

Synchrotron radiation, photofragment fluorescence spectroscopy and mass spectrometry were used to study the VUV photodissociation and dissociative photoionization of gaseous acetic acid in the 6–23 eV photoexcitation range. Earlier studies were limited to the region below 11.7 eV. We recorded the dispersed fluorescence spectra excited at six different energies between 10 and 20 eV. The emission observed corresponds to OH ($A^2\Sigma^+ \rightarrow X^2\Pi$), CH ($A^2\Delta \rightarrow X^2\Pi$), CH ($B^2\Sigma^- \rightarrow X^2\Pi$) and H-Balmer transition features. We studied the relative intensities of these emissions by fluorescence excitation (FEX) spectroscopy over the range 6–22 eV. No other emissions were observed, in particular none from the HCOO radical. The fluorescence and FEX spectra were analyzed and the photodissociation processes forming the emitting electronic states of OH, CH and H were determined with the aid of data from VUV absorption spectra, FEX onset energies and thermochemical limit calculations. We found that the fluorescence quantum yields for OH and CH emissions, which varied over the 6–22 eV region, were always less than 1%. The photoionization mass spectra (PIMS) of CH_3COOH were measured at $E_{exc} = 20$, 25 and 100 eV, and the ion yield curves were measured over the range 6–23 eV for the parent and principal fragment ions. Features in the ion yield curves were correlated with features in the absorption and photoelectron spectra, reflecting in part the opening up of access to various ion states of acetic acid. The appearance energies of the principal ionic products were determined from the ion yield curves and compared with the values derived from thermochemical calculations. Our measured ionization energy of acetic acid, IE (CH_3COOH) $= 10.58 \pm 0.02$ eV is 40–60 meV lower than previous PIMS values. Dissociative ionization reaction channels are discussed in detail and their validity checked with the aid of experimental and calculated appearance energies and with

their compatibility with the results of TPEPICO measurements, carried out by Zha et al. [5] at much greater energy intervals (150–250 meV) than in our experiments (30 meV). H atom loss from the parent ion was not observed. The major fragment ion is CH_3CO^+. Its measured appearance energy calls into question previous determinations of the heat of formation and ionization energy of the acetyl radical. The assignment of the $m/z = 31$ ion to CH_2OH^+ is confirmed. A new pathway is suggested for the formation of HCO^+, and the assignments of the $m/z = 16$ ion to CH_4^+ and the $m/z = 28$ ion to CO^+ are justified. The formation of the important CH_3^+ ion at threshold is shown to involve carbon–carbon bond rupture and a potential energy barrier. At higher energies CH_3^+ is also formed by a reaction involving initial formation of the acetyl radical cation. Some astrophysical implications of our results are discussed concerning acetic acid in the interstellar, cometary and meteoritic media.

Acknowledgements

We thank François Dulieu and Jean-Louis Chotin for their valuable assistance during the synchrotron radiation beam time periods. We are grateful for support from the European Commission programme "Access to Research Infrastructures" for providing access to the Berlin BESSY synchrotron facility under contract FMRX-CT-O126 and for access to the LURE Synchrotron Facility in Orsay. Welcome support from the CNRS Groupe de Recherche "GDR Exobiologie"(GDR 1877) and from INSU is gratefully acknowledged.

References

[1] R.S. Berry, S. Leach, Adv. Electron. El. Phys. 57 (1981) 1.
[2] M.B. Robin, Higher Excited States of Polyatomic Molecules, Academic Press, New York, 1975.
[3] M. Suto, X. Wang, L.C. Lee, J. Phys. Chem. 92 (1988) 3764.
[4] Ya.Ya. Villem, M.E. Akopyan, Russ. J. Phys. Chem. 50 (1976) 394.
[5] Q. Zha, T. Nishimura, M.J. Bertrand, G.G. Meisels, Int. J. Mass Spectrom. Ion Proc. 107 (1991) 515.
[6] D.M. Mehringer, L.E. Snyder, Y. Miao, F.J. Lovas, Astrophys. J. 480 (1997) L71.
[7] J. Crovisier, D. Bockelée-Morvan, P. Colom, N. Biver, D. Despois, D. Lis, Astron. Astrophys. 418 (2004) 1141.
[8] D.K. Harvey, K.J. Feierabend, J.C. Black, V. Vaida, J. Mol. Spectrosc. 229 (2005) 151.
[9] S. Leach, M. Schwell, S. Un, H.-W. Jochims, H. Baumgärtel, Chem. Phys. 321 (2006) 159.
[10] M. Schwell, F. Dulieu, H.-W. Jochims, J.-H. Fillion, J.-L. Lemaire, H. Baumgärtel, S. Leach, J. Phys. Chem. A 106 (2002) 10908.
[11] O. Braitbart, S. Tobita, S. Leach, P. Roy, I. Nenner, Am. Inst. Phys. Conf. Proc. 258 (1992) 42.
[12] T.A. Field, F. Dulieu, J.-H. Fillion, J.-L. Chotin, S. Douin, J.-L. Lemaire, S. Leach, Chem. Phys. 250 (1999) 81.
[13] L.C. Lee, M. Suto, Chem. Phys. 110 (1986) 161.
[14] S.S. Hunnicutt, L.D. Waits, J.A. Guest, J. Phys. Chem. 93 (1989) 5188.
[15] S.S. Hunnicutt, L.D. Waits, J.A. Guest, J. Phys. Chem. 95 (1991) 562.
[16] D.R. Peterman, R.G. Daniel, R.J. Horwitz, J.A. Guest, Chem. Phys. Lett. 236 (1995) 564.
[17] I.P. Vinogradov, F.I. Vilesov, Khim. Vys. Energ. 11 (1977) 25.
[18] NIST Chemistry Webbook (2005), National Institute of Standards and Technology Standard Reference Database. Available from: <http://webbook.nist.gov>.
[19] S.G. Lias, J.E. Bartmess, J.F. Liebmann, J.L. Holmes, R.D. Levin, W.G. Mallard, J. Phys. Chem. Ref. Data 17 (Suppl. 1) (1988).
[20] J.C. Traeger, B.M. Kompe, in: J.A. Martinho Simoes, A. Greenberg, J.F. Liebman (Eds.), Energetics of Organic Free Radicals, Blackie Academic and Professional, London, 1996, p. 59.
[21] B. Ruscic, M. Schwarz, J. Berkowitz, J. Chem. Phys. 91 (1989) 6780.
[22] E.H. Kim, S.E. Bradforth, D.W. Arnold, R.B. Metz, D.M. Neumark, J. Chem. Phys. 103 (1995) 7801.
[23] S.J. Blanksby, T.M. Ramond, G.E. Davico, M.R. Nimlos, S. Kato, V.M. Bierbaum, W.C. Lineberger, G.B. Ellison, M. Okumura, J. Am. Chem. Soc. 123 (2001) 9585.
[24] J.L. Holmes, F.P. Lossing, P.M. Mayer, J. Am. Chem. Soc. 113 (1991) 9723.
[25] K.P. Huber, G. Herzberg, Constants of Diatomic Molecules, Van Nostrand Reinhold, New York, 1979.
[26] T. Ari, H.H. Güven, J. Electron Spectrosc. Rel. Phen. 106 (2000) 29.
[27] M.C.R. Symons, J. Phys. Chem. 87 (1983) 1833.
[28] S.D. Peyerimhoff, P.S. Skell, D.D. May, R.J. Buenker, J. Am. Chem. Soc. 104 (1982) 4515.
[29] A. Rauk, D. Yu, D.A. Armstrong, J. Am. Chem. Soc. 116 (1994) 8222.
[30] P.H. Cannington, N.S. Ham, J. Electron Spectrosc. Rel. Phen. 31 (1983) 175.
[31] J. Berkowitz, Photoabsorption, Photoionization and Photoelectron Spectroscopy, Academic Press, New York, 1979, p. 245.
[32] A.N. Stepanov, A.A. Perov, S.P. Kabanov, A.P. Simonov, High Energy Chem. 22 (1986) 81.
[33] K.D. Cook, J.W. Taylor, Int. J. Mass Spectrom. Ion Phys. 30 (1979) 93.
[34] D.J. Knowles, A.J.C. Nicholson, J. Chem. Phys. 60 (1974) 1180.
[35] F. Carnovale, T.H. Gan, J.B. Peel, J. Electron Spectrosc. Rel. Phen. 20 (1980) 53.
[36] T. Nishimura, G.G. Meisels, Y. Niwa, J. Chem. Phys. 91 (1989) 4009.
[37] H.-W. Jochims, M. Schwell, J.-L. Chotin, M. Clemino, F. Dulieu, H. Baumgärtel, S. Leach, Chem. Phys. 298 (2004) 279.
[38] D.N. Shigorin, A.D. Filygina, V.K. Potapov, Teor. Eksp. Khim. 2 (1966) 417.
[39] M.A. Haney, J.L. Franklin, Trans. Faraday Soc. 65 (1969) 1794.
[40] J.C. Traeger, R.G. McLoughlin, A.J.C. Nicholson, J. Am. Chem. Soc. 104 (1982) 5318.
[41] J.L. Holmes, F.P. Lossing, J. Am. Chem. Soc. 102 (1980) 3732.
[42] M.C.R. Cockell, J.M. Dyke, H. Zamanpour, in: C.Y. Ng (Ed.), Vacuum Ultraviolet Photoionization and Photodissociation of Molecules and Clusters, World Scientific, Singapore, 1991, p. 43.
[43] D.F. McMillen, D.M. Golden, Ann. Rev. Phys. Chem. 33 (1982) 493.
[44] W. Tsang, in: J.A. Martinho Simoes, A. Greenberg, J.F. Liebman (Eds.), Energetics of Organic Free Radicals, Blackie Academic and Professional, London, 1996, p. 22.
[45] H. Schwarz, D.H. Williams, C. Wesdemiotis, J. Am. Chem. Soc. 100 (1978) 7052.
[46] D.J. McAdoo, C.E. Hudson, L.L. Griffin, J. Phys. Chem. 88 (1984) 1481.
[47] E.T.M. Selim, A.I. Helal, Ind. J. Pure Appl. Phys. 19 (1981) 977.
[48] K. Hirota, K. Nagoshi, M. Hatada, Bull. Chem. Soc Jpn. 34 (1961) 226.
[49] B. Ruscic, M. Litorja, Chem. Phys. Lett. 316 (2000) 45.
[50] A. Brack (Ed.), The Molecular Origins of Life, Cambridge University Press, Cambridge, UK, 1998.
[51] H.-W. Jochims, H. Baumgärtel, S. Leach, Astron. Astrophys. 314 (1996) 1003.
[52] M.P. Bernstein, S.F.M. Ashbourn, S.A. Sandford, L.J. Allamandola, Astrophys. J. 601 (2004) 365.
[53] W.H. Sorrell, Astrophys. J. 555 (2001) L129.
[54] W. Huntress, G. Mitchell, Astrophys. J. 231 (1979) 456.

[55] V. Blagojevic, S. Petrie, D.K. Bohme, Mon. Not. R. Astron. Soc. 339 (2003) L7.
[56] A. Remijan, L.E. Snyder, S.-Y. Liu, D. Mehringer, Y.-J. Kuan, Astrophys. J. 576 (2002) 264.
[57] T.H.B. Kuiper, in: M.P. van Haarlem (Ed.), Perspectives on Radio Astronomy – Science with Large Antenna Arrays, Netherlands Foundation for Research in Astronomy, 1999, p. 275.
[58] Y.-J. Kuan, S.B. Charnley, H.-C. Huang, W.-L. Tseng, Z. Kisiel, Astrophys. J. 593 (2003) 848.
[59] P. Thaddeus, M. Guélin, R.A. Linke, Astrophys. J. 246 (1981) L41.
[60] Y.C. Minh, M.K. Brewer, W.M. Irvine, P. Friberg, L.E.B. Johansson, Astron. Astrophys. 244 (1991) 470.
[61] C. Chyba, C. Sagan, Nature 355 (1992) 125.
[62] F. Henry, J. Crovisier, D. Bockelée-Morvan, H. Rauer, D. Lis, Astrophys. Space Sci. 277 (2001) 303.
[63] Y. Huang, Y. Wang, M.R. Alexandre, T. Lee, C. Rose-Petruck, M. Fuller, S. Pizzarello, Geochim. Cosmochim. Acta 69 (2005) 1073.
[64] J.R. Cronin, S. Chang, in: J.M. Greenberg, C.-X. Mendoza-Gomez, V. Pirronello (Eds.), The Chemistry of Life's Origins, Kluwer, 1993, p. 209.